

PULSAR POLARIZATION FLUCTUATIONS AT 430 MHz WITH MICROSECOND TIME RESOLUTION

J. M. CORDES

Department of Physics and Astronomy, University of Massachusetts, Amherst

AND

T. H. HANKINS

National Astronomy and Ionosphere Center, Arecibo Observatory

Received 1976 August 17; accepted 1977 May 26

ABSTRACT

This paper studies the polarization properties of pulsars 0950+08, 1133+16, 1919+21, and 2016+28 after the removal of interstellar dispersion distortion. Autocorrelation functions of the Stokes parameters were computed for narrow longitude regions and were summed to reduce statistical errors. Such autocorrelation functions quantify the mean-square properties of polarization fluctuations and reveal how the polarization decorrelates on time scales between the reciprocal receiver bandwidth ($8 \mu\text{s}$) and the maximum lag of 4 ms.

We find that single-pulse polarization is only partially correlated with the polarization of the average profile, where the latter is measured by synchronously averaging the Stokes parameters of many single pulses. Deviations of single-pulse polarization from the average are highly correlated with intensity fluctuations such as micropulses and subpulses. Ninety-degree transitions of the position angle, for example, can occur on the periphery of micropulses, just as slower 90° rotations sometimes occur on the edges of subpulses. Micropulses—seen from all except PSR 1919+21—are more polarized than the subpulses that contain them by as much as a factor of 2. We find for PSR 1133+16 that a change in sense of the circular polarization is usually coincident with a 90° transition of the position angle. Subpulses from PSR 1919+21 and PSR 2016+28 show a systematic advancement of the position angle at their leading edges relative to their trailing edges that may be due to preferential occurrence of ninety-degree angle rotations. Microstructure from PSR 1133+16 and PSR 2016+28 shows periodicities, with respective periods of 1.2 ms and 0.9 ms, that are more pronounced in the leading half of the average profile than in the trailing half. In general, the polarization and the strength of micropulses are strongly dependent on pulse longitude, while the average time scale is not.

We infer from the autocorrelation functions and from single pulses that the state of polarization is usually constant through a micropulse but may change rapidly (e.g., via a 90° angle transition and/or a sense change of the circular polarization) on the extremity of a micropulse or between two micropulses. Rapid polarization changes within some micropulses cannot be ruled out, but the strength and number of such micropulses must contribute negligibly to the autocorrelation functions.

Subject headings: polarization — pulsars

1. INTRODUCTION

Individual pulses from pulsars are typically highly polarized with linear polarization usually prevalent over circular polarization. The polarization state can vary both randomly and systematically within individual pulses as well as from pulse to pulse. Intrapulse fluctuations have been associated with subpulses (Taylor *et al.* 1971; Lyne, Smith, and Graham 1971; Rankin, Campbell, and Backer 1974; Manchester, Taylor, and Huguenin 1975) whose polarization is usually correlated, to some extent, with that of the average profile, although subpulses can be considerably more polarized than the average. The depolarization that usually occurs in the averaging process is due to the pulse-to-pulse fluctuations of the subpulses'

polarization state. Pulsars with drifting subpulses have depolarized averages because the polarization position angle rotates with respect to position in the subpulse rather than with respect to position in pulse longitude. Depolarization of the average can also come about because two preferred, orthogonal position angles may occur in subpulses at a given pulse longitude, a property first mentioned by Lyne *et al.* for PSR 1133+16 and more recently reported to be a property common to all 12 objects investigated by Manchester, Taylor, and Huguenin (1975). It has also been found that polarization position angles become more random with increasing radio frequency, thereby causing the decrease of average linear polarization that has been observed (Manchester, Taylor, and Huguenin 1975).

Another class of intensity fluctuations are micro-pulses (microstructure) which have been seen in about 80% of the pulsars investigated (Hankins, Rickett, and Cordes, in preparation). Micropulses have widths of a few tenths of a degree of longitude (where 360 degrees equals one pulse period) compared with subpulse and profile widths of a few degrees and one to a few tens of degrees, respectively.

Single-channel measurements indicate that micropulses, although usually occurring *within* subpulses, are in many ways like shorter-time-scale versions of subpulses. Micropulse time scales, for example, are not measurably frequency-dependent in the 74 to 430 MHz frequency range, just as subpulses are at most weakly frequency-dependent over the same range. Micropulses occur with random positions within subpulses just as subpulses have random positions within the mean pulse profile. However, for PSR 2016+28, a pulsar which has drifting subpulses that are periodically situated within a pulse, the microstructure can also occur quasi-periodically within the subpulses.

Except for the cursory observations by Craft, Comella, and Drake (1968), which showed the presence of circularly polarized microstructure from PSR 0950+08, no detailed analyses of microstructure polarization have been made.

The temporal resolution of microstructure requires a bandwidth that is sufficiently small that dispersion distortion does not obliterate the microstructure. Small bandwidths, however, result in considerable estimation error ($> 10\%$) if the microstructure time scale is not much larger (< 100 times) than the receiver resolution. Dispersion distortion can be removed, as for the data analyzed in this paper, by digital filtering (see Hankins 1971), but hardware considerations at present limit the bandwidth to 125 kHz if two polarization channels are recorded. The estimation error problem can be circumvented with no loss of time resolution by computing autocorrelation functions of pulse intensities and summing them to form an average. Analyses of this kind have been performed on single-channel data (Hankins 1972; Cordes and Hankins 1973; Cordes 1976*a*), and in this paper we shall discuss the autocorrelation functions (acf's) of the Stokes parameters. In a separate paper (Cordes 1976*b*, hereafter Paper I) a formalism is developed for evaluating polarization parameters from the acf's. A particular advantage of the acf technique is that it permits measurement of polarization fluctuations that occur over a range of time scales, including sample-to-sample variations with $8 \mu\text{s}$ time scales. The usual technique of studying the smoothed Stokes parameters has a resolution equal to the postdetection smoothing time, which is usually a large fraction of a millisecond.

II. DATA PROCESSING

The four pulsars were observed in 1975 May and June and 1976 April by using the 305 m telescope and the 430 MHz line feed at the Arecibo Observatory (NAIC). The 430 MHz line feed provides left- and right-hand circular polarizations (LHCP and RHCP)

with a cross-coupling coefficient of the power in each channel of less than 0.25% (Rankin, Campbell, and Spangler 1975). The intermediate-frequency signals, whose bandwidths were 125 kHz, were mixed to base-band (i.e., centered on zero frequency) and digitally recorded before detection at $8 \mu\text{s}$ intervals during a 50 to 80 ms window that was centered on the phase of the average pulse profile. The data were subsequently processed to remove distortion caused by interstellar dispersion, the details of which may be found in Hankins (1971). Removal of dispersion distortion yields a time resolution equal to the reciprocal receiver bandwidth, or $8 \mu\text{s}$.

Stokes parameters were computed from the dispersion-free signals according to standard definitions (e.g., Kraus 1966). Denoting the undetected signals from each receiver as $v_{i,r}(t, k)$ for sample number t of the k th pulse and the corresponding intensities as $I_{i,r}(t, k) = |v_{i,r}(t, k)|^2$, the *unsmoothed* Stokes parameters of the k th pulse are

$$I(t, k) = I_l(t, k) + I_r(t, k)$$

$$V(t, k) = I_l(t, k) - I_r(t, k)$$

$$L(t, k) = Q(t, k) + iU(t, k) = 2v_l(t, k)v_r^*(t, k). \quad (1)$$

Average Stokes parameter profiles, such as those found in the literature (Komesaroff, Morris, and Cooke 1970; Lyne, Smith, and Graham 1971; Rankin, Campbell, and Backer 1974; Manchester, Taylor, and Huguenin 1975), were computed by summing the Stokes parameters of individual pulses:

$$\begin{aligned} \langle I(t) \rangle &= N^{-1} \sum_{k=1}^N I(t, k), \\ \langle V(t) \rangle &= N^{-1} \sum_{k=1}^N V(t, k), \\ \langle L(t) \rangle &= N^{-1} \sum_{k=1}^N L(t, k). \end{aligned} \quad (2)$$

The Stokes parameters of individual pulses contain an enormous quantity of information, much of which is lost in the computation of the mean profiles. In order to extract some of this information and, at the same time, reduce the large estimation errors of the unsmoothed single-pulse Stokes parameters, the autocorrelation functions of the Stokes parameters were computed. The single-pulse acf of the total intensity, for example, was computed according to

$$R_I(\tau, k) = T^{-1} \sum_{t=1}^T I(t, k)I(t + \tau - 1, k), \quad (3)$$

where $\tau = 1, \dots, \tau_{\text{max}} = 512$. The average acf was computed according to

$$R_I(\tau) = \sum_k R_I(\tau, k), \quad (4)$$

a sum which weights each individual acf by the mean-square intensity of the pulse. Similar acf's were computed for V and L , except that the lagged value of L was complex-conjugated before taking the product. The acf of L was computed, rather than separate acf's for Q and U , because Q and U both measure linear polarization with their relative values directly related to the polarization angle ψ by

$$\psi = 0.5 \tan^{-1}(U/Q). \quad (5)$$

Thus L is a vector in the complex plane whose magnitude measures the degree of linear polarization and whose angle equals the longitude of the polarization state in the Poincaré sphere. If L makes large excursions about the complex plane, its average will be small compared with instantaneous values. The acf of L measures the relative magnitude and angle on the complex plane of values of L separated by the time interval τ .

Autocorrelation functions were normalized according to

$$r_I(\tau) = R_I(\tau)/R_I(0), \quad r_V(\tau) = R_V(\tau)/R_V(0), \\ r_L(\tau) = R_L(\tau)/R_L(0), \quad (6)$$

rather than self-normalizing all acf's according to, e.g., $r_V(\tau) = R_V(\tau)/R_V(0)$. The chosen normalization is useful because the correlation coefficients $r_V(\tau)$ and $r_L(\tau)$ become proportional to the mean-square degree of circular and linear polarization and therefore satisfy

$$r_V(\tau) + |r_L(\tau)| \leq r_I(\tau), \quad (7)$$

where equality holds if the signal is completely polarized in a time-independent polarization state. Equality always holds for $\tau = 0$ because

$$Q^2 + U^2 + V^2 = I^2 \quad (8)$$

is an identity for unsmoothed Stokes parameters.

In practice, acf's were obtained by fast Fourier transform techniques whereby the autocorrelation, which is the convolution of the signal with its time-reversed conjugate, was computed by multiplication of transforms in the frequency domain. Frequency-domain products for individual pulses were summed to obtain the transform of the average acf, which was then inverse-transformed to obtain the average acf. Transforms of length 1024 yield 512 lags of the acf. Time series of arbitrarily long lengths can be processed in this fashion by breaking the series into 1024 sample blocks separated by 512 samples (see Bergland 1969). Rader (1970) has shown how to optimize the processing by constructing 1024 point transforms of the data from 1024 point transforms of 512 data points and 512 zeros. Also, for real data, two Fourier transforms can be computed simultaneously by letting one block of data represent the real part, the other block the imaginary part, of a fictitious block of complex data; the transforms of the two blocks are easily unwoven. By these methods, data-processing time was approxi-

mately 1/10 of that required for direct time-domain computations. A final step in improving the efficiency of the data processing involved the deletion of pulse periods in which there was no emission. PSR 0950+08 and PSR 1133+16 frequently show type I nulls (Backer 1970), about one in every 10 to 20 pulses, when the pulsar apparently "turns off" for one to a few pulse periods.

Errors in the Stokes parameters arise from gain differences between the two channels, from deviations of the feed from circular polarization, and from unbalanced base-band mixers. In the Appendix it is shown that such instrumental effects cause, at most, errors of 5% in the autocorrelation functions. Errors in the Stokes parameters themselves are less than 10%, an amount that is determined primarily by cross-coupling of polarized power between the LHCP and RHCP ports of the line feed. In the Appendix it is shown that cross-coupling cannot cause the observed correlation of 90° jumps of the polarization angle with zero crossings of the circular polarization (see § III).

Another practical detail is the correction of the acf's for system and sky noise, which contributes primarily to the zero-lag values of the acf's if the mean off-pulse intensities are subtracted from the data before acf processing. The following quantities must be subtracted from the zero-lag values of the unnormalized acf's:

$$C_I = C_V = (1 + 2\langle I_{\text{ron}} \rangle / \langle I_{\text{roff}} \rangle) \langle I_{\text{roff}} \rangle^2 \\ + (1 + 2\langle I_{\text{lon}} \rangle / \langle I_{\text{loff}} \rangle) \langle I_{\text{loff}} \rangle^2 \\ C_L = 4(\langle I_{\text{loff}} \rangle \langle I_{\text{roff}} \rangle + \langle I_{\text{ron}} \rangle \langle I_{\text{loff}} \rangle + \langle I_{\text{lon}} \rangle \langle I_{\text{roff}} \rangle) \quad (9)$$

where $\langle I_{l, \text{ron, off}} \rangle$ are the mean on- and off-pulse intensities for the LHCP and RHCP channels. Estimation errors of the off-pulse corrections, which are inversely proportional to the square root of the number of data points used in the estimation, can cause normalization errors in the acf's. Such errors are always less than a few percent.

Faraday rotation in the ionosphere and the interstellar medium can depolarize the linear polarization, but at 430 MHz the differential angle rotation over a 125 kHz bandwidth is less than 1° for a maximum rotation measure of 50 rad m⁻². No calculation of absolute position angles was made because only relative angles were of interest.

The acf's were block smoothed over five samples (not including the zero-lag spike) in order to reduce the estimation error; the resolution of the acf's is thus 40 μs.

III. RESULTS

Mean Stokes parameter profiles for each pulsar (Fig. 1) were computed from the same pulses used for the acf processing. Although the estimation errors of the profiles are evident owing to the small number of pulses used in the computation, the profiles are consistent with those published by Manchester (1971). The profiles were segmented into longitude regions, as

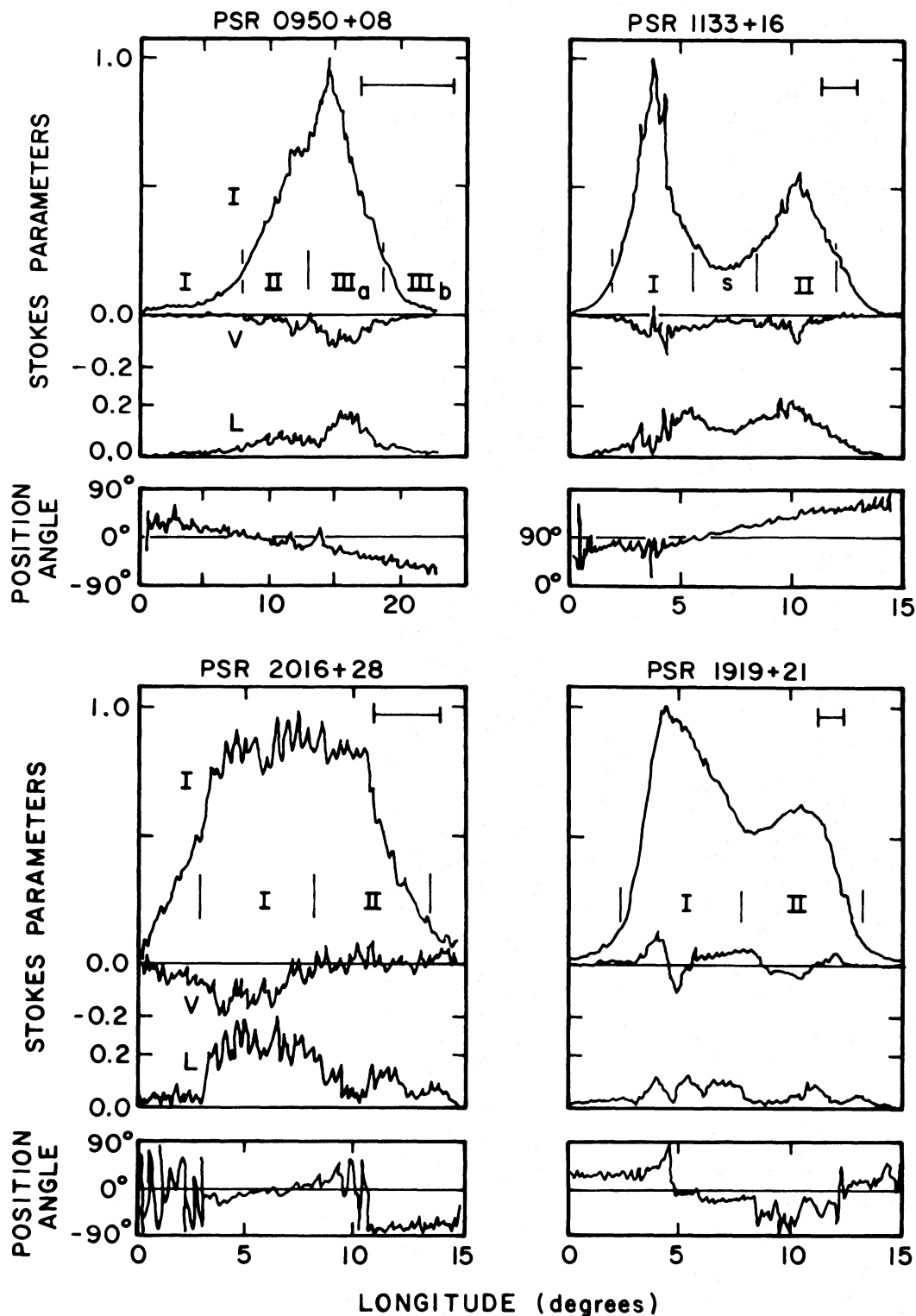


FIG. 1.—Average Stokes parameter profiles for four pulsars at 430 MHz obtained by summing the Stokes parameters of 130 to 200 pulses. The total intensity (I), the circular polarization (V), the linear polarization (L), and the position angle are defined in § II. The position angles are *not* absolute. A horizontal bar represents 5 ms of time. Time resolution is 256 μ s. Estimation errors range between a few and 10%; the largest is for PSR 2016+28, which has drifting subpulses and strong micropulses that contribute to the noise in the Stokes parameters.

designated in Figure 1, on the basis of polarization structure in the profiles and on the basis of fluctuation-spectral properties reported by Backer (1973). Mean values of d_V and d_L , the degrees of circular and linear polarization, were calculated for each longitude region according to, e.g.,

$$\langle d_V \rangle = \frac{\int dt \langle V(t) \rangle}{\int dt \langle I(t) \rangle} \quad (10)$$

and are tabulated in Table 1. Autocorrelation functions of the Stokes parameters were computed separately for each longitude region of each pulsar; the results appear in Figures 2 to 5.

The autocorrelation functions contain zero-lag spikes—features that decorrelate on an inverse-bandwidth ($8 \mu\text{s}$) time scale whose heights are related to the integrated mean-square values of d_V and d_L . The

remainder of the acf's contain features that correspond to subpulses and micropulses, both of which contribute to the second moments of the Stokes parameters. In general, individual pulses are more highly polarized than the average profiles because fluctuations of the polarization state, which arise in complicated ways from subpulse and (if present) micropulse polarization fluctuations, depolarize averages of many pulses. Similarly, micropulses are more polarized than subpulses because the polarization state varies from micropulse to micropulse but can be more stable within a micropulse. Thus the features in the acf's corresponding to subpulses and micropulses, which are identifiable by their different time scales, will show different levels of polarization.

An empirical model that is developed in Paper I provides the means for evaluating polarization parameters from the acf's. The model represents subpulses as

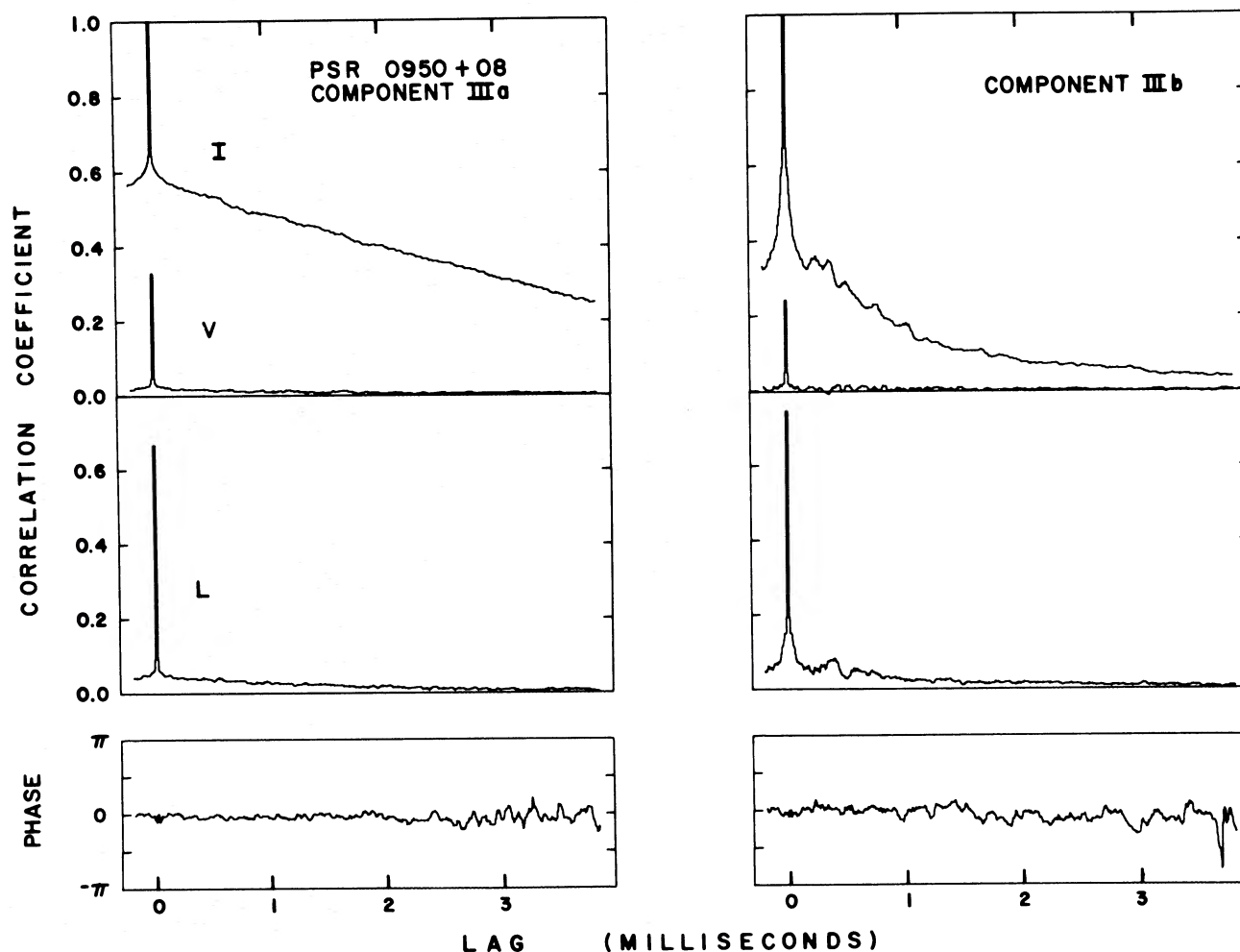


FIG. 2.—Average autocorrelation functions (acf's) of the Stokes parameters for PSR 0950+08, computed by summing acf's of 157 single-pulse Stokes parameters. The acf's of the total intensity (I) and the circular polarization (V) are real, whereas the acf of the linear polarization (L) is complex, and for which we show the magnitude and the phase. Except for the zero-lag spikes, the acf's are smoothed over $40 \mu\text{s}$. The microstructure time scale is $\sim 170 \mu\text{s}$, and it is clear that microstructure is stronger in the trailing edge of the average profile (component III_b) than in the center (component III_a).

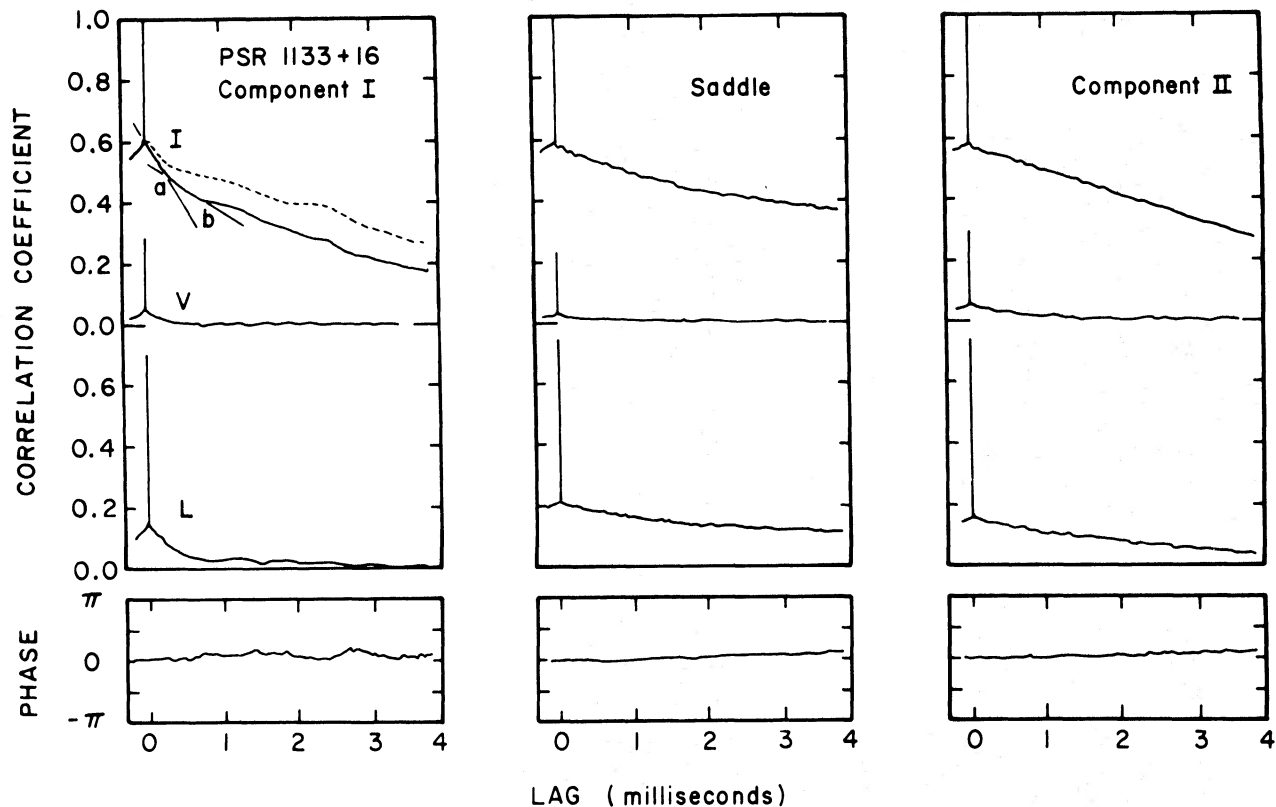


FIG. 3.—Average autocorrelation functions as in Fig. 2 for 278 pulses from PSR 1133 + 16; acf's are shown for components I and II and the interlying saddle region of the average profile. Microstructure is most evident in component I, where points *a* and *b* designate two break points in the microstructure portion of the acf corresponding to time scales of 350 and 800 μ s, respectively. The dashed curve is the intensity acf for an independent set of 100 pulses in which the break point at *b* is not present.

nonstationary stochastic modulations (*S*) of stationary microstructure (μ)

$$A(t) = S(t)\mu(t). \quad (11)$$

The average pulse profile could be included as a further modulation in equation (11) (see Rickett 1975), but for our purposes we consider it to be lumped into *S*(*t*). Because μ (*t*) is stationary, its acf can be put in the form

$$r_{\mu}(\tau) = [1 + m_{\mu}^2 \rho_{\mu}(\tau)] / (1 + m_{\mu}^2), \quad (12)$$

where M_{μ} is the modulation index of microstructure defined by

$$m_{\mu}^2 = \langle \mu^2 \rangle / \langle \mu \rangle^2 - 1, \quad (13)$$

and $\rho_{\mu}(\tau)$ is the autocovariance of μ (the acf of $\mu - \langle \mu \rangle$) with $\rho_{\mu}(0) = 1$. The width of ρ_{μ} is a measure of the average microstructure correlation time. Under the assumption that polarization fluctuations and intensity fluctuations are statistically independent, the acf of *I* can be written as (we denote with a bar an acf which excludes the zero-lag spike, that feature which decorrelates on a time scale equal to the inverse

receiver bandwidth, or 8 μ s)

$$\bar{r}_i(\tau) = 2r_s(\tau)r_{\mu}(\tau)/(3 + \langle d^2 \rangle), \quad (14)$$

where $d^2 \equiv d_v^2 + d_L^2$ is the total degree of polarization and $r_s(\tau)$ is the acf of *S*(*t*).

Similarly, we write the acf's of *V* and *L* as

$$\begin{aligned} \bar{r}_v(\tau) &= \bar{r}_i(\tau)R_{d_v}(\tau) \\ \bar{r}_L(\tau) &= \bar{r}_i(\tau)R_{d_L}(\tau) \exp(i\phi_L(\tau)) \end{aligned} \quad (15)$$

where R_{d_v} and R_{d_L} are the acf's of d_v and d_L . The phase ϕ_L of the acf of *L* is related to random and systematic fluctuations of the polarization angle because R_L is the sum of many terms of the form

$$\begin{aligned} L_0(t, k)L_0(t + \tau - 1, k) \\ \times \exp\{2i[\psi(t, k) - \psi(t + \tau - 1, k)]\} \end{aligned} \quad (16)$$

where L_0 is the magnitude of *L*.

The zero-lag values of R_{d_v} and R_{d_L} measure the sample-to-sample level of polarization which is also the maximum microstructure polarization. At a lag where the microstructure fluctuations are decorrelated,

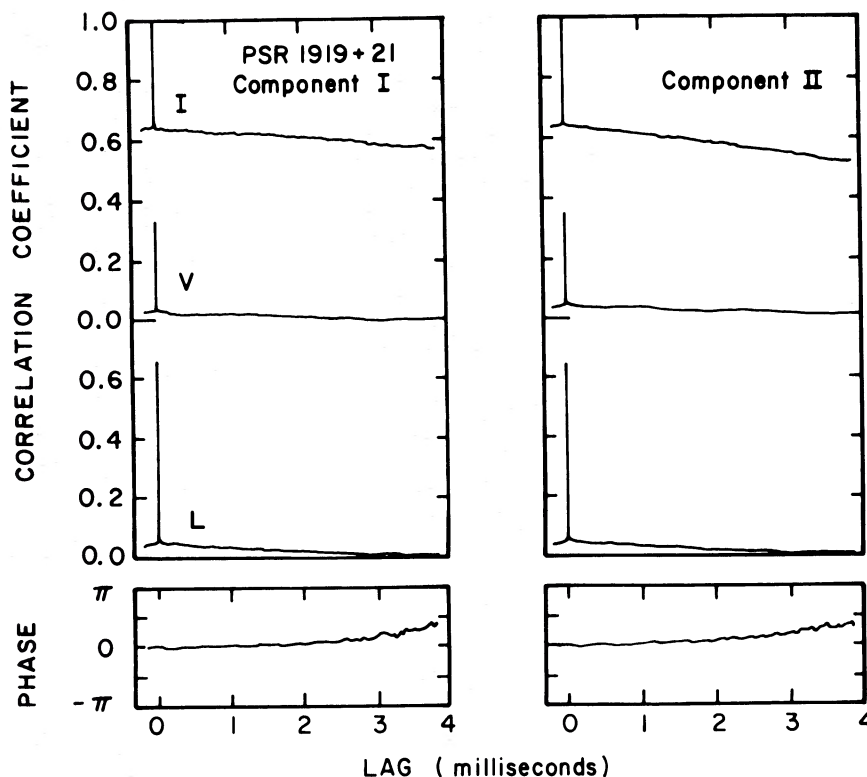


FIG. 4.—Average autocorrelation functions as in Fig. 2 for 206 pulses from PSR 1919 + 21. There is no evidence of microstructure in either component, and subpulses are evidently weakly polarized. The increase of the phase of the acf of L starting at a lag of about 3 ms suggests that the position angle on the leading edge of a subpulse is systematically advanced with respect to the angle at the trailing edge.

the levels of polarization are those associated with subpulses. We shall consider a lag, τ_μ , such that $\rho_\mu(\tau_\mu) = 0$ but $\rho_\mu(\tau_\mu^-) > 0$. Evaluation of the acf's at lags $\tau = 0$ and $\tau = \tau_\mu$ enables us to solve for the following six quantities:

$$\begin{aligned} \langle d^2 \rangle &= 2\bar{r}_I(0)^{-1} - 3 = (|\bar{r}_L(0)| + \bar{r}_V(0))/\bar{r}_I(0), \\ \langle d_{V^2} \rangle_\mu &= \bar{r}_V(0)/\bar{r}_I(0) \\ \langle d_{L^2} \rangle_\mu &= |\bar{r}_L(0)|/\bar{r}_I(0) \\ \langle d_{V^2} \rangle_S &= \bar{r}_V(\tau_\mu)/\bar{r}_I(\tau_\mu) \\ \langle d_{L^2} \rangle_S &= |\bar{r}_L(\tau_\mu)|/\bar{r}_I(\tau_\mu) \\ m_\mu^2 &= \bar{r}_I(0)\bar{r}_S(\tau_\mu)/\bar{r}_I(\tau_\mu) - 1. \end{aligned} \quad (17)$$

If the polarization state were time-independent, then the microstructure and subpulse degrees of polarization, $\langle d_{V,L^2} \rangle_\mu^{1/2}$ and $\langle d_{V,L^2} \rangle_S^{1/2}$, would be equal to the degree of polarization of the average profile, $\langle d_{V,L} \rangle$. Generally, however, the micropulse polarization will be greater than the subpulse polarization, which, in turn, will be greater than the polarization of the average profiles.

The assumption that polarization and intensity fluctuations are independent is not a critical one—it is merely an artifice for easily quantifying the features in

the acf's. If the assumption does not hold, the average quantities expressed in equations (17) can be re-expressed as integrals of those quantities weighted by the instantaneous intensity.

The two equalities in the first of equations (17) yield two estimates for $\langle d^2 \rangle$ whose difference, if any, is due to normalization errors of the acf's; values of $\langle d^2 \rangle^{1/2}$ in Table 1 include error limits that are based on this difference. Estimation of τ_μ , in practice, involves a subjective judgment as to where the microstructure feature of the acf's drops to zero. Usually a roughly parabolic-shaped curve was sketched over the acf's to estimate $r_S(\tau)$, and the intersection of the curve with a straight line drawn tangent to the microstructure feature was used to estimate τ_μ . Errors of τ_μ and m_μ listed in Table 1 reflect the accuracy of this procedure. Along with the six quantities expressed in equations (17) is tabulated the stability of the linear polarization at 410 MHz obtained from Manchester, Taylor, and Huguenin (1975). The stability, which in our notation is

$$\sigma = |\langle L \rangle|/|\langle L \rangle|, \quad (18)$$

indicates how the linear polarization of the average profile is depolarized due to pulse-to-pulse fluctuations of the polarization angle. Tabulated values of σ were obtained by averaging over the longitude region of

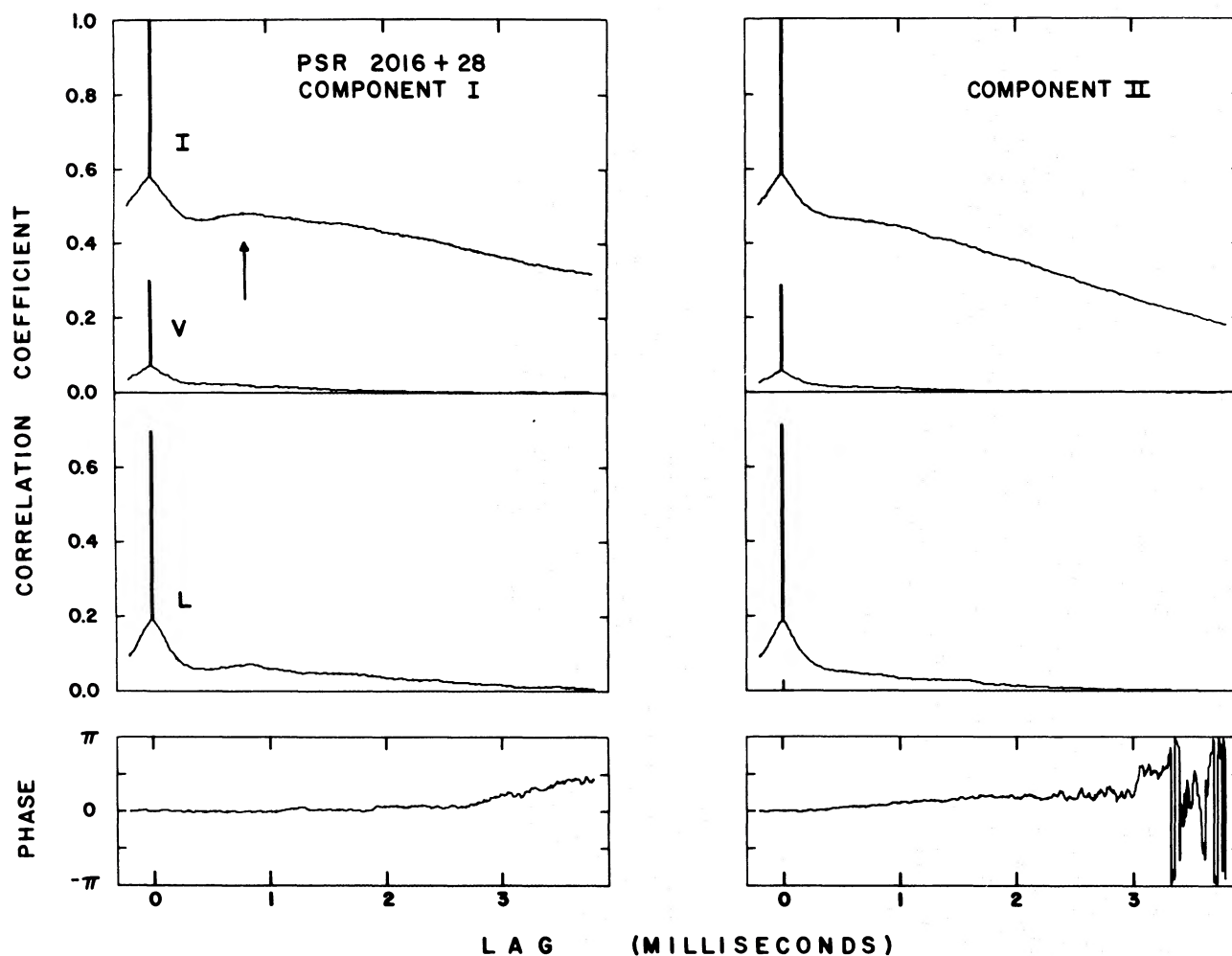


FIG. 5.—Average autocorrelation functions as in Fig. 2 for 286 pulses from PSR 2016+28. The microstructure time scale is $290 \mu\text{s}$ in both components. An arrow designates an enhancement that corresponds to a quasi-periodicity in the microstructure, of which a $900 \mu\text{s}$ period is the most common.

interest. The results for each pulsar will now be individually discussed.

a) PSR 0950+08

Above a frequency of about 300 MHz, the double lobes of the average profile of PSR 0950+08 have merged to form a structure which has three identifiable longitude regions, as delineated in the Stokes parameter profiles of Figure 1. The center of the pulse, which marks the boundary of components II and III, is weakly polarized ($\sim 10\%$) compared with the $\sim 50\%$ polarization in the wings of the profile. Manchester, Taylor, and Huguenin (1975) attribute this dip in linear polarization to the occasional presence of subpulses at this longitude whose position angles are orthogonal to the angle expected by extrapolation from neighboring longitudes. Emission in component I actually extends 150° of longitude to the interpulse,

with the polarization angle rotating continuously through the whole longitude region (Lyne, Smith, and Graham 1971).

Autocorrelation functions, which were computed only for components II and III because the small signal-to-noise ratio in component I causes large estimation errors, show marked longitude dependence in the strength and polarization of microstructure, while the microstructure time scale remains constant at $\sim 170 \mu\text{s}$. Polarization parameters in Table 1 indicate that the modulation index, which quantifies the contribution of microstructure to the mean-square intensity, is greater in component III_b than in components II and III_a by a factor of ~ 3.5 . Micropulses are only about 10% more polarized than the subpulses that contain them. Subpulses in component III_b, which has a large stability (0.9), are only slightly more polarized than the average profile. By contrast, regions II and III_a, which have stabilities of 0.6 and 0.5, respectively,

TABLE 1
PULSAR POLARIZATION PROPERTIES AT 430 MHz

PSR	COMPONENT	MEAN PROFILE		SUBPULSES			MICROSTRUCTURE				NOISE $\langle d^2 \rangle^{1/2}$	COMMENTS
		$\langle d_t \rangle$	σ	$\langle d_V \rangle_S^{1/2}$	$\langle d_L \rangle_S^{1/2}$	$\Delta\phi_S$	$\langle d_V \rangle_\mu^{1/2}$	$\langle d_L \rangle_\mu^{1/2}$	$\Delta\phi_\mu$	m_μ		
0950+08.....	II	-0.06	0.17	0.20	0.34	...	0.24	0.34	...	0.22	160	0.42
	III _a	-0.09	0.11	0.18	0.28	30°	0.24	0.32	15°	0.24	170	0.4
	III _b	-0.22	0.40	0.13	0.45	65°	0.20	0.51	20°	0.82	170	0.55
1133+16.....	I	-0.09	0.13	0.16	0.25 (0.34)	60°	0.29	0.50	15°	0.68 (0.48)	370,700*	0.57
	Saddle	-0.17	0.52	0.17	0.60 (0.53)	5°	0.21 (0.27)	0.64	5°	0.27 (0.21)	325,750*	0.67
	II	-0.08	0.41	0.18 (0.32)	0.48	5°	0.27 (0.36)	0.52	5°	0.30	325,860*	0.59
1919+21.....	I	0.05	0.10	0.20	0.30	25°	0.36
	II	-0.003	0.08	0.24	0.27	30°	0.36
2016+28.....	I	-0.13	0.27	0.29	0.45	20°	0.41	0.63	5°	0.54	290	0.75
	II	+0.02	0.12	0.13	0.35	45°	0.32	0.59	10°	0.47	300	0.67

NOTES:—The quantity σ is the stability, ranging between 0 and 1, of the linear polarization, as defined in equation (18). A value of unity means that successive pulses have identical linear polarization. $\Delta\phi_s$, $\Delta\phi_\mu$ are the peak-to-peak fluctuations in the phase of the acf of L in the subpulse and the micropulse regions of the acf, respectively. Errors in the degrees of polarization are $\pm 5\%$. Errors in the microstructure modulation index, m_μ , are $\pm 5\%$. Errors in the micropulse time scale, τ_μ , are $\pm 5\%$, except for values marked with an asterisk which have $\pm 10\%$ errors. For PSR 1133+16, quantities in parentheses apply to the case when the longer-time-scale microstructure is absent. Parenthetical values are given only if they differ significantly from those when the longer-scale microstructure is present.

show subpulses that are twice as polarized as the average profile but are less linearly polarized than the subpulses in component III_b.

b) PSR 1133 + 16

The polarization properties of the average profile, a well-resolved double lobe, show notable differences between component I and the rest of the profile. The first component shows small ($\sim 10\%$) linear polarization, compared with 40%–70% polarization in com-

ponents S and II, because the polarization angle undergoes frequent transitions between two orthogonal angles from pulse to pulse and because the subpulses in individual pulses are intrinsically less polarized. Manchester, Taylor, and Huguenin (1975) reported that approximately 25% of the subpulses in component I have position angles that are orthogonal to the angle expected by extrapolating the angle rotation elsewhere in the pulse. The stability of the polarization angle is accordingly much smaller in component I than in the saddle region and component II.

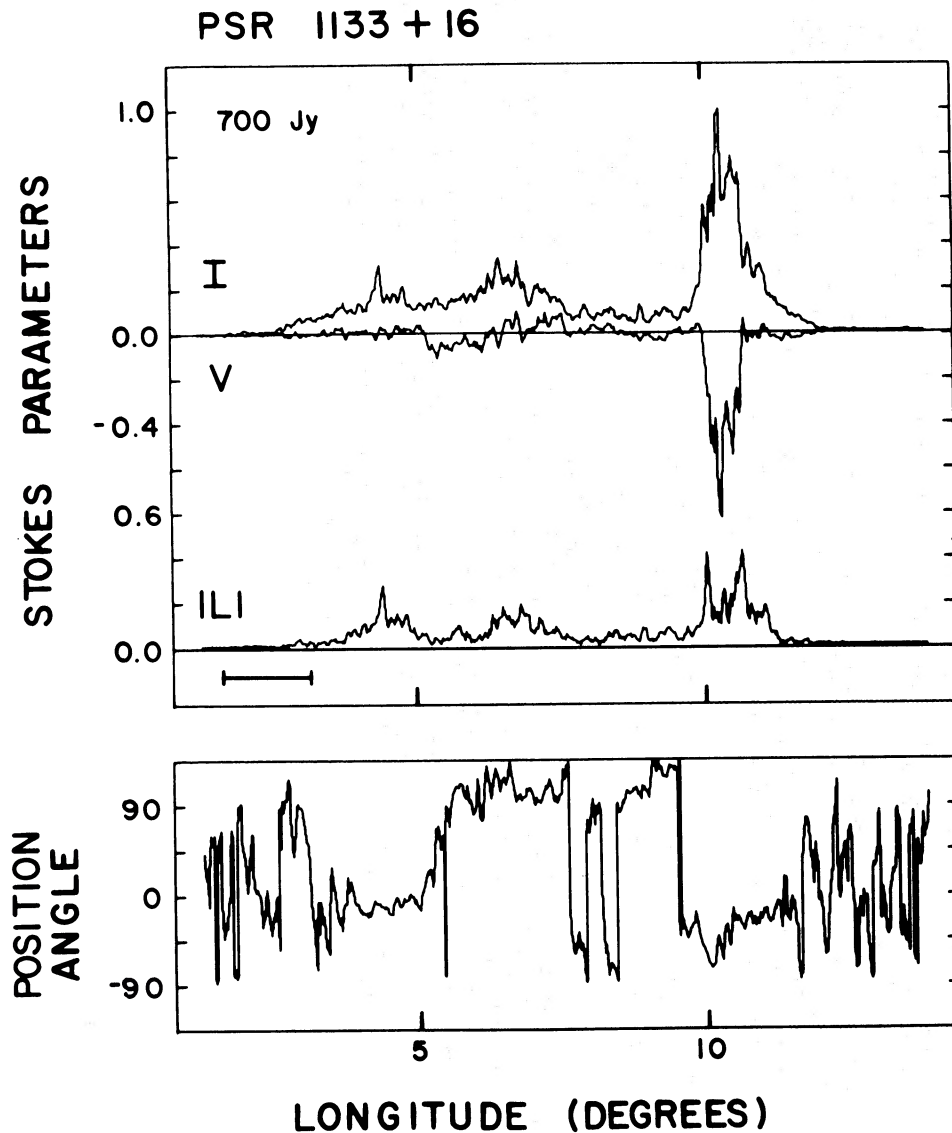


FIG. 6.—The Stokes parameters of single pulses from PSR 1133 + 16 are plotted with $256 \mu\text{s}$ resolution in time (0.078 of longitude) corresponding to estimation errors that are 12.5% of the local mean. A negligible amount of error is caused by receiver and sky noise except on the right and left extremities of the figures, where the pulsar intensity is low and the polarization angle becomes uniformly distributed over $\pm 90^\circ$. Jumps of 180° in the position angle are nonphysical and are due to the wraparound ambiguity of the arctangent function. The flux density of the pulse peak is shown in janskys ($10^{-26} \text{ W m}^{-2} \text{ Hz}^{-1}$) to a precision of $\pm 20\%$. The horizontal bar represents 5 ms of intrapulse time. (a) An amorphous pulse with strong emission in the saddle region with little obvious microstructure. The position angle rotates through 90° over a time of 2 ms at a longitude of $\sim 5^\circ$.

Two kinds of pulses can be identified in a set of pulses. One has subpulses with amorphous internal structure which sometimes includes micropulses that are not particularly well defined. These pulses often show strong subpulses in the saddle region as well as in components I and II. The polarization state in amorphous pulses, two examples of which are shown in Figures 6a and 6b, is usually stable with the angle rotating slowly through the pulse as in the average profile of Figure 1. Frequently in component I and less often in component II, however, the angle can undergo a 90° rotation over a few milliseconds' time interval on the periphery of subpulses, sometimes accompanied by a change in sense or increase of

circular polarization. Such 90° rotations, which were first noted by Lyne *et al.*, are evident in Figure 6. The other kind of pulse, which we call "spiked," has subpulses that are confined to a narrow range of pulse longitude, usually in component I or II, that have well-defined micropulses. Pulses of the second kind are usually several times more intense than those of the first kind. As may be seen from examples in Figures 6c and 6d, transitions of the position angle can occur over a short time interval (100–200 μ s) on the periphery of micropulses and are almost always accompanied by changes in the sense of circular polarization. Micropulse boundaries and sense changes of the circular polarization seem to be necessary but not sufficient

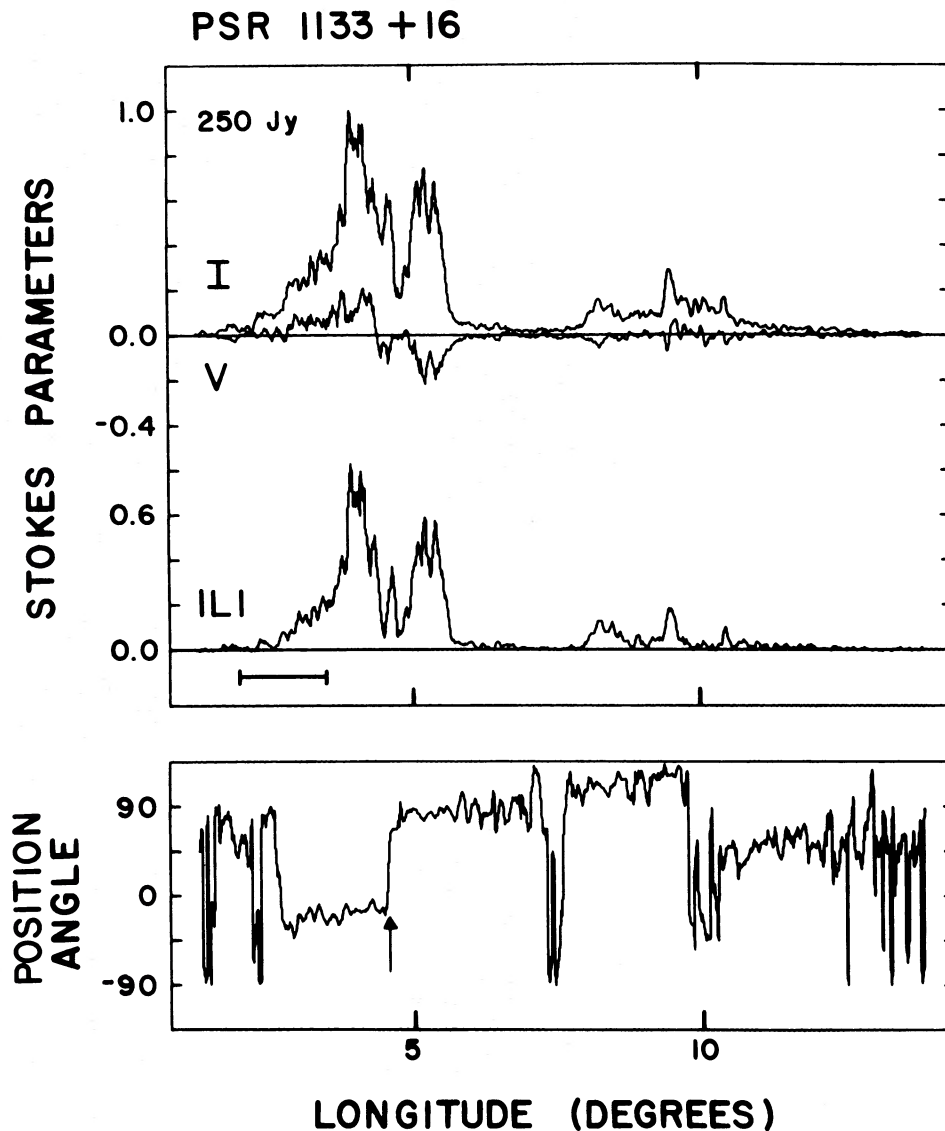


FIG. 6b.—An amorphous pulse with a 90° transition of the position angle (arrow) and a reversal of the circular polarization between two micropulses in component I. The transition time is on the order of 200 μ s. The position angle rotates fairly continuously, following that of the average profile in Fig. 1, until it makes a downward transition of 90° near a longitude of 10° .

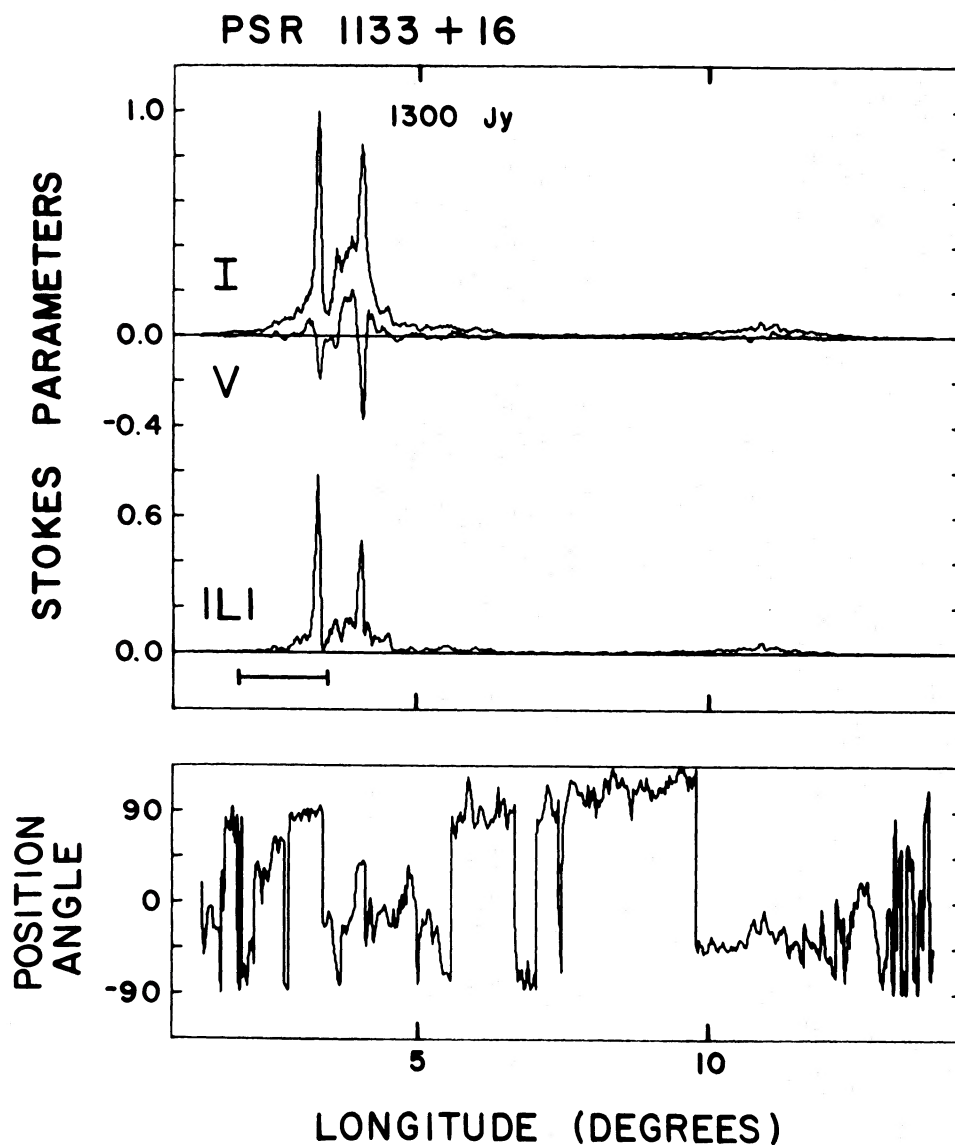


FIG. 6c.—A strong “spiked” pulse with prominent micropulses within a subpulse that is confined to a narrow range of longitude in component I. A considerably weaker subpulse appears in component II and there is emission in the saddle region, evidenced by the nonrandom position angle there. Several sense changes of the circular polarization occur in component I along with erratic (and possibly 90°) jumps of the position angle. These angle jumps are probably statistically significant because the signal-to-noise ratio is high (~ 900) for the peak intensity and, as discussed in the text, the position angle is usually steady over the duration of a micropulse, as it appears here.

co-occurrences of these “fast” transitions of the angle because subpulses with micropulses can have stable angles across a subpulse, as in Figure 6d. In general, however, the polarization angle and circular polarization appear constant for each micropulse, but the angle can vary in component I both randomly and orthogonally with respect to adjacent micropulses.

If we refer to the acf's in Figure 3 for the three components, it is evident that microstructure contributes much more to intensity variations in component I than elsewhere in the pulse. Indeed, the microstructure modulation index is greater by a factor

of 2.4 in component I than in the saddle region and in component II. The microstructure feature in component I has two break points at lags of $340 \mu\text{s}$ and $600\text{--}900 \mu\text{s}$; acf's for different sets of pulses reveal that the longer-time-scale microstructure is not always present—or, more accurately, that its contribution to the second moment of the intensity varies considerably. The microstructure modulation index is $\sim 25\%$ smaller when the longer-time-scale microstructure is absent, suggesting that it is associated with the intense, spiked subpulses.

It is possible that the appearance of spiked subpulses

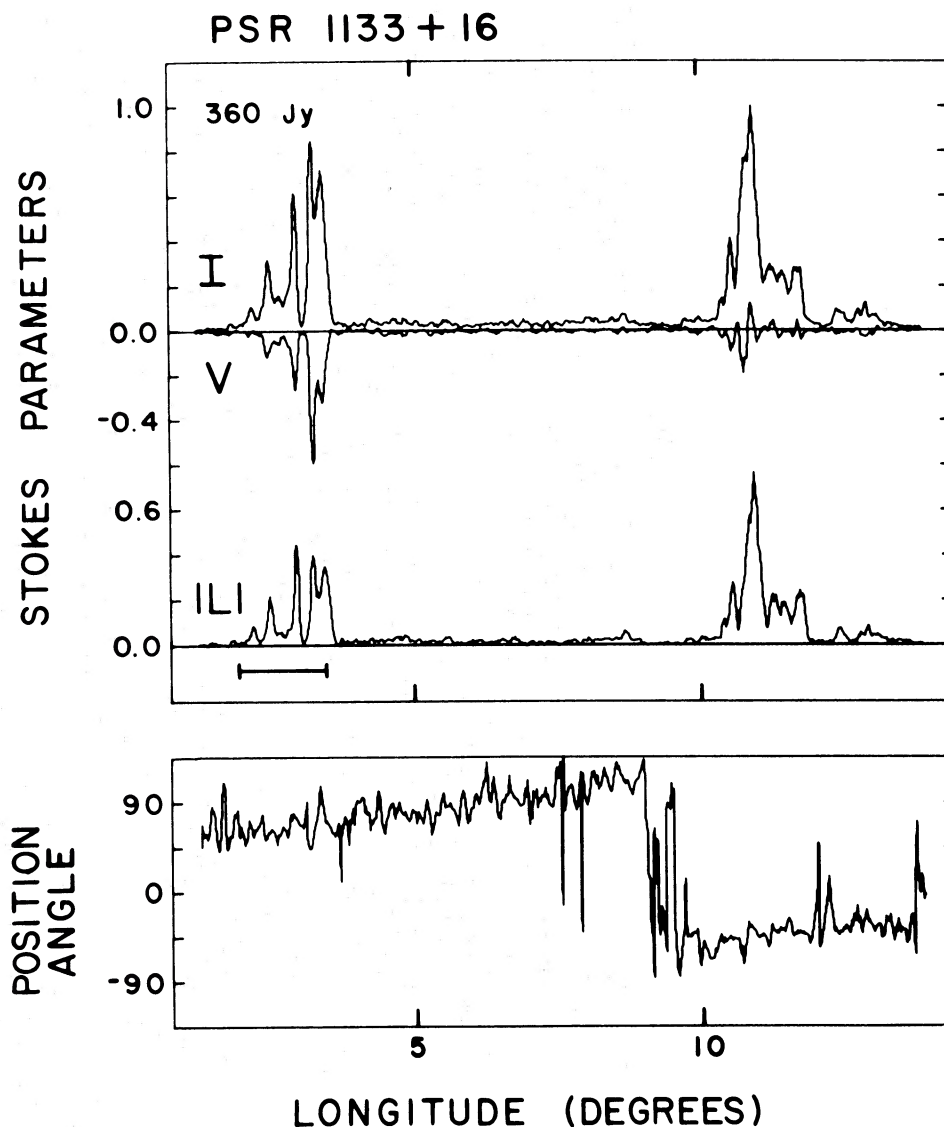


FIG. 6d.—A pulse with “spiked” subpulses in both components I and II and with low-level emission in the saddle region. In component I there are no significant sense changes of the circular polarization *and* no jumps in the position angle, which rotates continuously through pulse longitude even though the circular polarization changes sign (possibly not statistically significant) in component II.

with hyperduration micropulses is connected with the mode behavior suggested by Helfand, Manchester, and Taylor (1975), in which the character of the average profile changes over 8 to 16 pulse periods. Intense subpulses with more than 5 times the integrated energy of the average subpulse occur about once in every 10 to 20 pulse periods, however, suggesting that true switching between modes is not occurring but, rather, that the long tail of the pulse energy distribution influences the stability of the average pulse profile.

Previous measurements of the micropulse time scales (Hankins 1972) attributes a value of $575 \mu\text{s}$ to the width of the autocorrelation feature at 111, 196, and 318 MHz. It is possible that these features, on closer inspection, also show dual microstructure time

scales. Clarification of this ambiguity is important because the frequency dependence of the microstructure time scale is critical to an understanding of its physics.

The acf's of component I differ from those of the other components also in the appearance of periodicities in the acf of I with a period of 1.2 ms. Analyses of separate data sets show that the periodicity does not always occur; and it is not clear whether the periodicity is due to only a few intense micropulses in a few subpulses or is truly an average effect. The facts that there are two cycles of the periodicity in the acf, however, and that the periodicity is evident in more than one data set, indicate that there is a systematic preference for micropulse separations of 1.2 ms.

Finally, the appearance of the periodicity in the acf of L indicates that adjacent periodic micropulses have partially correlated polarization states.

Regarding polarization, we see from the acf's that micropulses are about equally polarized in all three longitude regions at about 50%–60% linear polarization. The linear and circular polarization decorrelate considerably on the micropulse time scale in component I, in contrast to the slow decorrelation in the other two components. The subpulse degree of linear polarization has an rms value that is twice as large in the saddle region and component II as in component I. It is clear, then, that in component I polarization variations on the micropulse time scale depolarize a subpulse if the subpulse is smoothed to the point of obliteration of the microstructure (as with the observations of Manchester, Taylor, and Huguenin 1975).

The behavior of the phase of r_L also distinguishes the polarization character of component I from the rest of the profile. In components S and II the phase shows only a small increase with increasing lag; there is little systematic deviation from a straight line. The small increase of phase with lag is directly related to the approximately linear rotation of the position angle in the average profile (Fig. 1). In component I the phase shows ripples with 45° peak-to-peak amplitudes and time scales about equal to the microstructure time scale, behavior which is undoubtedly related to random or 90° jumps of the position angle between micropulses. The phase is comparatively constant under the microstructure portion of the acf, again indicating that the polarization state is constant over a micropulse duration.

c) PSR 1919+21

PSR 1919+21 shows complicated variation of the polarization state through the average profile. The average degrees of polarization are small (~10%) in the two components. Fast changes in the polarization state occur at various longitudes, particularly near the first peak of the average profile, where the linear polarization drops nearly to zero, the sense of circular polarization changes, and there is a 60° change in the position angle (Fig. 1). These particular features are coincident with a longitude region where drifting subpulses are strong and the discontinuous change in the polarization state may very well be related to the deep notch in the average profile seen at frequencies below about 200 MHz (Hankins 1973; Cordes 1975).

The acf's for components I and II are similar, showing no sign of microstructure and indicating that individual pulses are weakly polarized (~35%). The phase of r_L in Figure 4 shows a nonlinear increase that begins at about a 3 ms lag. Its appearance in both components suggests that it is a property of the drifting subpulses rather than of the mean pulse profile. Cordes (1975) showed that the dominant pulse constituent at 430 MHz is nondrifting and extends over nearly the whole longitude range of the average profile. Drifting subpulses have widths of about 2.5 ms

that correspond to an autocorrelation half-width of about 3.5 ms. The acf's of V and L are approximately that wide, suggesting that the polarization is associated with the drifting subpulses whose relatively small contribution to the total intensity accounts for the low percentage of polarization. Unpublished data from Rankin (1973) indeed show that the polarization is correlated with the drifting subpulses as for PSR 0809+74 and PSR 0031-07 (Taylor *et al.* 1971; Manchester, Taylor, and Huguenin 1975).

The systematic increase of the phase of r_L beginning at about a 3 ms lag implies a systematic variation of the position angle through a subpulse, possibly due to the presence of orthogonal position angles on opposite sides of the subpulses. At lags between 3 and 4 ms, it is just those portions of the subpulses that contribute to the lagged products of the acf's. That the phase increases with lag implies that the position angle at the leading edge of a subpulse is advanced with respect to the angle at the trailing edge.

d) PSR 2016+28

The average Stokes parameters for this object (Fig. 1) show that the leading and trailing edges are weakly polarized while a broad region in the front part of the pulse is more highly polarized with $\langle d_V \rangle \approx -0.15$ and $\langle d_L \rangle \approx 0.30$. The position angle slowly rotates through the region of high polarization, undergoes a 90° transition at the trailing edge of the region, and then appears to be constant.

This object displays drifting subpulses that contain well-defined micropulses (Backer 1973; Boriakoff 1976; Cordes 1976a). Manchester, Taylor, and Huguenin (1975) state that the polarization drifts with the subpulses, as for PSR 0031-07 and PSR 0809+74, with the position angles of the leading and trailing edges of the subpulses usually being at mutually orthogonal angles. The microstructure has a quasi-periodic component with period $P_\mu \approx 0.9$ ms that is dominated in its contribution to the intensity variance by an aperiodic component.

If we refer to the acf's for components I and II in Figure 5 and to Table 1, it is evident that the microstructure modulation index, the strength of the microstructure periodicity (which appears as a correlation enhancement at a lag of about 0.9 ms), and the degrees of linear and circular polarization are all larger in component I than in component II. Values of m_μ in the two components, 0.54 and 0.47, are consistent with a value of 0.50 presented in a previous work (Cordes 1976a) that was obtained from an acf computed over the whole longitude region of the pulse profile. The microstructure periodicity is barely discernible in component II, but the period in both components is the same as that reported previously (Boriakoff 1976; Cordes 1976a). In component I, the periodicity appears in the acf of L as well as in the acf of I . It follows that neighboring *periodic* micropulses share the same linear polarization state. Generally, however, the polarization state is substantially decorrelated between micropulses because micropulses are 40% and

70% more polarized than subpulses in components I and II, respectively.

As with PSR 1919+21, the phase of r_L begins to increase nonlinearly at a lag (~ 3 ms) that corresponds to subpulse widths. The sense of the phase change again indicates that the position angles of the leading edges of subpulses are systematically advanced with respect to the trailing edges, possibly by the 90° rotations reported by Manchester, Taylor, and Huguenin (1975). Wiggles in the phase of r_L suggest that, as for component I of PSR 1133+16, there are large variations of the position angle between micropulses. Ninety-degree transitions are indeed evident in

Figure 7, which shows a single pulse which comprises two subpulses.

IV. DISCUSSION

a) Micropulses and Subpulses

The polarization exhibited in single pulses—i.e., that associated with subpulses and micropulses—evidently can be described as one of the following two forms: (1) a slow variation of the polarization state across pulse longitude that is similar to that of the integrated Stokes parameters; or (2) occasional rapid transitions of the polarization state between two orthogonal

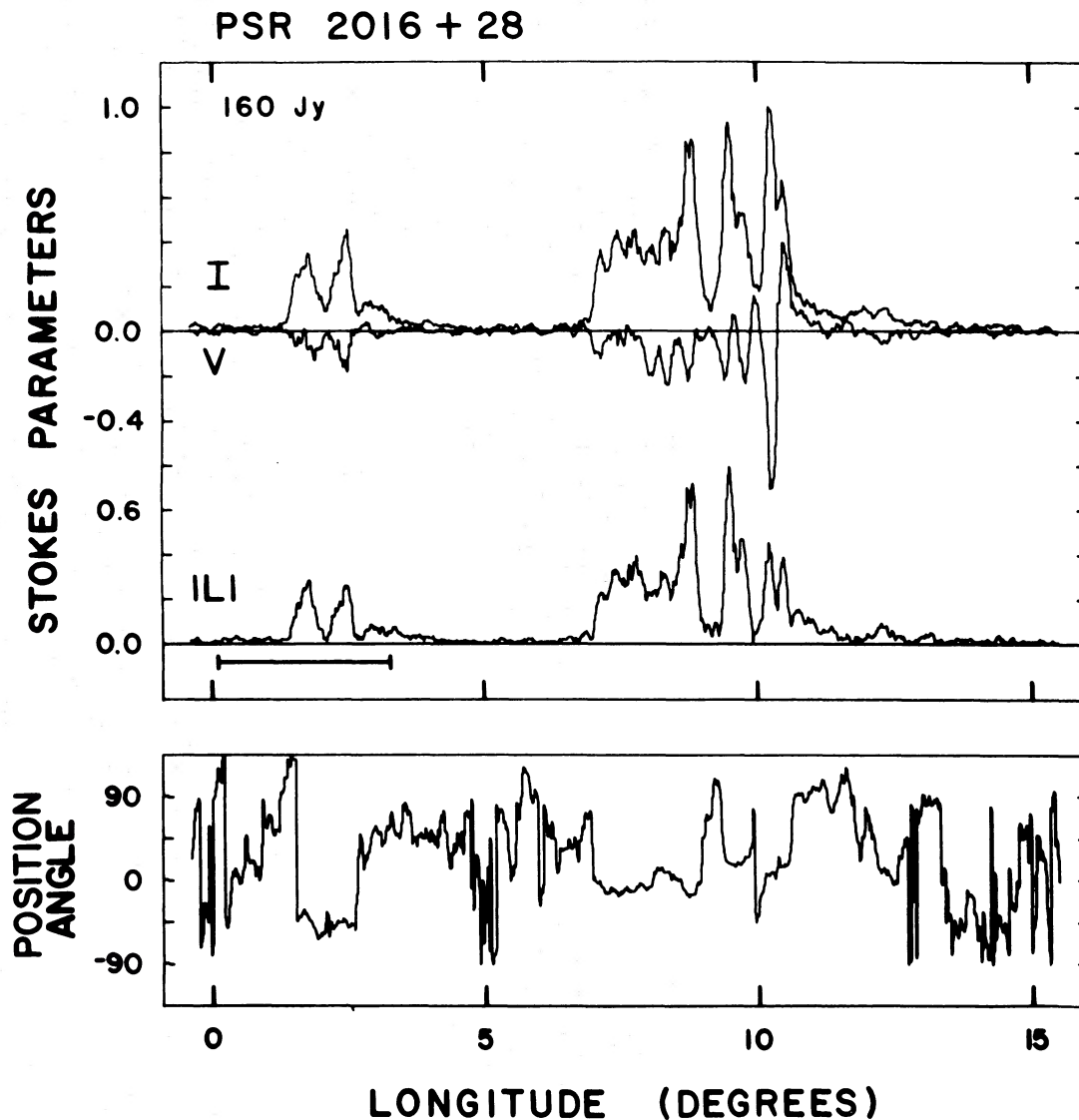


FIG. 7.—The Stokes parameters of a single pulse from PSR 2016+28 plotted with $256 \mu\text{s}$ time resolution or 0.165° longitude resolution. The horizontal bar represents 5 ms of time. See legend of Fig. 6 for other comments. The emission from this pulsar is in the form of drifting subpulses, two of which are evident here separated by about 10 ms of time or 6.5° longitude. The position angle is extremely erratic, even where the signal-to-noise ratio is large (the ratio is ~ 110 for the peak intensity). As we have found from the autocorrelation functions of the Stokes parameters and as is evident here, the state of polarization is essentially constant over the duration of a micropulse but can change drastically on the edge of a micropulse.

states which have position angles separated by 90° and have opposite senses of circular polarization. We have found that transitions between orthogonal states of polarization preferentially occur on the edges of subpulses and micropulses, while the polarization remains roughly constant (i.e., it obeys case [1] above) over most of the duration of a subpulse or a micropulse. Polarization transitions do not always occur, however; but when they do, they tend to be on the boundaries of subpulses and micropulses.

b) Digression on Micropulse Polarization

The tendency for fast polarization changes to occur primarily on the boundaries of micropulses can be demonstrated from the shapes of the autocorrelation functions. We warn, however, that individual micropulses may or may not conform to the polarization behavior deduced from autocorrelation functions; acf's are dominated by the larger-amplitude and/or broader micropulses because each micropulse's contribution to an acf is weighted by its mean-square intensity. Occasional large-amplitude pulses from PSR 1133+16 can have total energies that are a factor of 10 or more greater than the mean energy; these pulses probably dominate the acf's for this pulsar. PSR 2016+28, however, shows little variation of micropulse variance and total pulse energy from pulse period to pulse period; acf's for this pulsar are therefore indicative of the behavior of most individual micropulses.

Referring to the acf's for PSR 1133+16 and PSR 2016+28 in Figures 3 and 5, we compare the shapes of the acf's for the three polarization quantities, I , V , and L . Specifically, we note that (1) the micropulse features in the acf's of V and L have the same width as that in the acf of I ; (2) the micropulse features are generally taller (relative to the flatter subpulse regions of the acf's) than the feature in the acf of I . The heights of the micropulse features are determined by how extensively the relevant quantity decorrelates; widths depend on the time scale of decorrelation. Restating points (1) and (2), we generalize that the linear and circular polarization of micropulses decorrelate to a greater extent than the total intensity, *but on the same time scale*. Such decorrelation can be explained by rapid transitions of the polarization state if they occur primarily on the edges of micropulses. If transitions occurred well within a micropulse, the micropulse features in the acf's of V and L would be narrower than that in the acf of I . On the other hand, if the state of polarization decorrelated *only* on time scales larger than the characteristic micropulse scale, then point (2) above would not be true: instead, the height of the micropulse feature relative to the subpulse level of the acf would be the same in the acf's of V and L as in the acf of I .

Concluding, we state that the Stokes parameters V and L of micropulses are not related to the micropulse intensity by a simple proportionality constant. The proportionality factor evidently changes by considerable amounts over a time scale that is short compared

with the micropulse width. When the factor changes, it does so preferentially on the boundaries of micropulses as opposed to in their interiors.

V. CONCLUSIONS

Our aim in this paper has been to explore the properties of pulsar radiation on short time scales; the ultimate goal is to identify processes in the pulsar magnetosphere that are responsible for what we observe. We have characterized the observed radiation as a stochastic sequence of polarization states, with structure in this sequence having several characteristic time scales. We therefore identify three morphological constituents in single pulses. *Subpulses* and *micropulses* may be considered envelopes of a *random noise process* whose fluctuation time scale is defined by the receiver bandwidth. The random noise process for PSR 2016+28 has Gaussian statistics (Cordes 1976a). Its intrinsic bandwidth may extend to a few GHz if micropulses themselves are due to broad-band sources. Of the three constituents, we must regard the noise as the most fundamental because its fluctuation time scale—perhaps as small as a nanosecond—is closest to that expected from an elemental radiation source. Micropulses and subpulses are presumably produced by grouping such elemental units together in large enough numbers that Gaussian statistics result.

Radhakrishnan and Cooke (1969) first proposed that coherent radiation is due to streaming charges that radiate by virtue of their motion along curved magnetic field lines. Assuming that the relevant field lines are near the magnetic pole of an approximately dipolar field, the features of the model follow: (1) a prediction that the polarization position angle rotates monotonically through the average pulse profile; the total angle swept ($\leq 180^\circ$) is determined by the minimum angle between the magnetic pole and the line of sight; (2) an association of spectral cutoffs of pulsars with the length scale over which particles radiate coherently; this length scale may be the size or spacing of particle "bunches" or it may be associated with maser amplification; in either case, radiation is relativistically beamed parallel to the particle momenta such that narrow (nanosecond duration) pulses are directed toward the observer (Paper I); (3) an understanding of the stability of polarization profiles of many pulse averages over periods of years if the stellar magnetic field dominates the formation of the radiation (Manchester *et al.* 1973).

Pulsar radiation deviates in several ways from the Radhakrishnan and Cooke model (viz., item [1] in preceding paragraph). Many pulsars show position angle rotations in average profiles that are non-monotonic and discontinuous (Manchester 1971; Rankin, Campbell, and Backer 1974), but it has been demonstrated (Backer, Rankin, and Campbell 1976) that such behavior can be understood simply by allowing a single pulse at a given longitude to have one of two preferred orthogonal position angles. The preferred angles, which are revealed in histograms of the position angle, each rotates smoothly with longitude

in a manner that is consistent with the Radhakrishnan and Cooke model. Other phenomena that need to be reconciled with the Radhakrishnan and Cooke model are: (1) the marked deviation of single-pulse polarization from the average polarization; (2) occasionally large percentages of circular polarization; and (3) a level of polarization on the $8 \mu\text{s}$ time scale (see § III) that is well below 100% polarization (Table 1).

Single-pulse polarization may deviate from the average polarization simply because of switching between orthogonal polarization states. Switching occurs preferentially on the boundaries of micropulses and subpulses, although switching certainly does not always occur, nor can we state that it occurs *only* on the boundaries. At observation frequencies near the upper end of the pulsar spectrum, polarization position angles become increasingly more random (Manchester, Taylor, and Huguenin 1975), indicating some process that further depolarizes pulsar radiation but is different from the more systematic switching between orthogonal states.

Curvature radiation from an ensemble of independent emitters is unlikely to produce substantial circular polarization. Opposite senses of circular polarization are radiated into directions that are on opposite sides of the trajectory plane of the particles. Radiation from a single emitter (a bunch or a plasma oscillation) will probably possess little circular polarization because particles will span different field lines, causing opposite senses of circular polarization to be added. More important, over the $8 \mu\text{s}$ resolution of our data, our line of sight will have sampled a region that contains many coherent emitters whose net circular polarization is equally likely to be positive or negative.

Total observed polarization on the $8 \mu\text{s}$ time scale, which we have called the "noise" level of polarization, is determined by depolarization that occurs on time scales of $8 \mu\text{s}$. If the polarization position angle is determined solely by the ambient magnetic field, we would expect to measure near-unity values for the noise level of polarization; this follows because the change in field line orientation (and hence the change in position angle) over the light distance corresponding to $8 \mu\text{s}$ is insufficient to account for the observed amount of depolarization. Depolarization over $8 \mu\text{s}$ may conceivably be caused by submicrosecond structure—which may also display 90° position angle transitions and circular polarization changes—that is averaged together by our receiver.

To account for such polarization phenomena, radiative-transfer effects probably have to be amended to the Radhakrishnan and Cooke model. Transitions

of the position angle between orthogonal angles may be intrinsic to the emission process, as suggested by Manchester, Taylor, and Huguenin (1975), who linked transitions with the polarization-dependent optical depths of a relativistic medium. Alternatively, position angle transitions may be imposed after emission, as with the Faraday pulsation model (Cocke and Pacholczyk 1976) or with induced scattering (Blandford and Scharlemann 1976). More work is clearly needed to describe the precision of any relationship between the intensity and the state of polarization. The preference for polarization transitions to occur on boundaries of micropulses and subpulses suggests that low-intensity regions have different polarization states than high-intensity regions. However, it is not clear why transitions do not always occur on pulse edges if the intensity is below some threshold value.

As for the viability of a postemission process being responsible for polarization transitions, we can state that our results disfavor arbitrary processes which treat the radiation as a perturbation of the responsible medium. The Faraday pulsation mechanism, for example, cannot explain the tendency for position angle transitions to occur on the edges of micropulses. Moreover, it predicts that position angle transitions occur when the circular polarization reaches a maximum, rather than when it makes a zero crossing. Evidently, the actual mechanism "knows" where micropulse boundaries are; it must therefore either be a feature of the emission mechanism or a postemission process where the pulse of radiation has sufficient energy to alter, in a time-dependent way, the medium through which it passes. A mechanism of this latter kind, known as self-induced transparency, explains the propagation of large-amplitude, pulsed, coherent, laser radiation with anomalously low dissipation through a medium with which the radiation is at resonance (McCall and Hahn 1969).

We thank B. J. Rickett for many helpful discussions. J. M. C. also thanks E. Tademaru for enlightening discussion and L. Pitchford for pointing out the self-induced transparency mechanism. J. M. C. thanks the National Astronomy and Ionosphere Center, Arecibo Observatory, for a Visiting Research Assistantship during which some of the data acquisition and analysis were performed. Arecibo Observatory is operated by Cornell University under contract with the National Science Foundation. This research was also supported by the NSF through grants MPS 71-03377 at the University of California and MPS 75-03377 at the University of Massachusetts. This paper is Contribution Number 230 of the Five College Observatories.

APPENDIX

INSTRUMENTAL POLARIZATION EFFECTS

Errors in polarization measurements derive from a number of sources in the receiver system, including cross-coupling of power between two orthogonal feeds, unequal gains in two receiver channels, and imperfect base-band mixers. Here we derive the errors which result from each of these sources of imperfection.

In general, if the actual left- and right-hand circularly polarized components of the electric field are

$$\mathbf{E} = \begin{pmatrix} E_r \\ E_l \end{pmatrix}, \quad (\text{A1})$$

then we can represent the measured receiver voltages before detection as

$$\mathbf{V} = \begin{pmatrix} v_r \\ v_l \end{pmatrix} = \mathbf{G}\mathbf{A}\mathbf{E} \quad (\text{A2})$$

where \mathbf{G} is a diagonal gain matrix with (real) elements g_r and g_l and \mathbf{A} is a unitary matrix which describes the cross-coupling (with magnitude and phase) between the two channels; that \mathbf{A} is unitary (i.e., the inverse of \mathbf{A} is equal to its conjugate transpose) implies that the norm of E , which is the power in the signal, is conserved. The transformation described by \mathbf{G} does not in general conserve power.

I. CROSS-COUPLING

Considering for now that \mathbf{G} is a unit matrix, we can show (e.g., Rankin, Campbell, and Spangler 1975) that the transformation described by \mathbf{A} separately conserves both the total measured power and the total polarized power, but linearly polarized power can be transformed into circularly polarized power and vice versa. If $L = Q + iU$, V are the "true" Stokes parameters of the field incident on the telescope, and L' , V' are the measured ones, then the errors in the measured parameters are

$$\Delta V' = 2(\alpha)^{1/2} \cos(\phi + 2\psi)|L| \quad (\text{A3})$$

$$\Delta L' = -2(\alpha)^{1/2} e^{i\phi} V \quad (\text{A4})$$

where $L = Q + iU$, $\psi = \tan^{-1}(u/Q)$ is the position angle of the source, α is the cross-polarized power between the two receiver channels, and ϕ is the phase of the cross-coupling. It is clear from equations (A3) and (A4) that a 100% linearly polarized signal can be converted by an imperfect antenna into an elliptically polarized signal whose state of polarization is a function of the position angle of the source.

Note that if the true polarization position angle were to jump by 90° ($\psi \rightarrow \psi \pm 90^\circ$), then the error in V would change sign [$\cos(\phi + 2\psi) \rightarrow -\cos(\phi + 2\psi)$]. Similarly, a change in sign of true circular ($V \rightarrow -V$) will appear as a 90° change in position angle of $\Delta L'$. Such spurious sign changes in the circular and 90° transitions in the position angle have a limiting amplitude given by $2(\alpha)^{1/2}$. Rankin, Campbell, and Spangler (1975) place an upper limit of $\alpha \leq 0.0025$ on the cross-polarized power between two circularly polarized ports of the 430 MHz line feed at Arecibo based on radar measurements on the planet Venus. Therefore we have the limits

$$|\Delta V'|/|L| \lesssim 0.1,$$

$$|\Delta L'|/|V| \lesssim 0.1. \quad (\text{A5})$$

If we take the view that 90° position angle transitions *induce* the observed zero crossings of the Stokes parameter V , then we require that the degree of circular polarization be at most 10% of the linear polarization on either side of the transition. Moreover, whenever there is a 90° transition there *must* be a zero crossing of the circular polarization if the transition is between angles such that $\cos(\phi + 2\psi)$ is not small. There are numerous counterexamples against these two phenomena for PSR 2016+28. The degree of circular polarization is sometimes more than 100% of the degree of linear polarization; zero crossings of V sometimes occur when there is no 90° angle transition; finally, the variation of the magnitude of V with pulse longitude is often much different from that of $|L|$ when the position angle is constant over longitude [for a variety of pulses with different constant position angles; i.e., $\cos(\phi + 2\psi)$ is not fortuitously zero for this phenomenon to occur], implying that the circular polarization is in general *not* related by a proportionality factor to the linear polarization. We conclude that cross-coupling is not responsible for the sometimes observed cooccurrence of 90° angle transitions and zero crossings of the Stokes parameter V .

Estimates of the mean degree of circular or linear polarization will be in error by the amounts

$$\langle d_L' \rangle - \langle d_L \rangle \approx -2(\alpha)^{1/2} \langle d_V \rangle \cos(\phi + 2\psi),$$

$$\langle d_V' \rangle - \langle d_V \rangle \approx 2(\alpha)^{1/2} \langle d_L \rangle \cos(\phi + 2\psi), \quad (\text{A6})$$

where unprimed and primed fractional polarizations are, respectively, the true and measured values.

Autocorrelation functions of V and L will be in error due to cross-coupling, but the acf of I will be unchanged. It can be shown that the autocorrelation function of the measured linear polarization (L') is of the form

$$r_{L'}(\tau) \approx (1 - 2\alpha)r_L(\tau) + 4\alpha r_V(\tau) + 8(\alpha)^{1/2} \int dt \langle I(t) \rangle^2 \langle d_V(t) \rangle \langle d_L(t) \rangle \cos[2\psi(t)] \Big/ \int dt \langle I(t) \rangle^2 (3 + \langle d(t) \rangle^2) \quad (\text{A7})$$

for small lags (i.e., lags less than the microstructure decorrelation time). The maximum magnitude for the last term is 0.05 when $\alpha = 0.0025$ and when $d_v = d_L = 2^{-1/2}$, $d = 1$, and $\psi = \text{constant}$. However, $d_v(t)$ and $\cos [2\psi(t)]$ will both change sign with time, so the result of the time integration will be a greatly diminished contribution from this term; conceivably, if $d_v(t)$ and $\cos [2\psi(t)]$ change sign together (which they do when sense changes of the circular polarization and 90° position angle contributions occur together), then the integration would not lessen the value of the term; however, the data indicate that $\psi(t)$ and $d_v(t)$ can change sufficiently independently that we can assign a value of zero to this term. For $\alpha = 0.0025$, the errors in $r_L(\tau)$ are on the order of 1%, a maximum value.

II. GAIN ERRORS

When the gains of the receiver channels are not identical, the measured Stokes parameters will be (primes)

$$\begin{aligned} I' &= GI + \Delta GV \\ L' &= gL \\ V' &= \Delta GI + GV, \end{aligned} \quad (\text{A8})$$

where $G = (g_i^2 + g_r^2)/2$, $\Delta G = \frac{1}{2}(g_i^2 - g_r^2)$, and $g = g_i g_r$. It can be shown that the resultant acf's will be

$$\begin{aligned} r_i'(0^+) &\approx r_i(0^+) [1 + 2\epsilon d_v(1 - d^2)/(3 + d^2)] \\ r_v'(0^+) &\approx r_v(0^+) [1 - 2\epsilon(3 + d^2 - 4d_v)/d_v(3 + d^2)] \\ r_L'(0^+) &\approx r_L(0^+) [1 + 8\epsilon d_v/(3 + d^2)], \end{aligned} \quad (\text{A9})$$

where we have used $g_{i,r} = 1 \mp \epsilon/2$.

For the measurements discussed in this paper, the gains were measured to an accuracy such that $|\epsilon| \leq 0.02$; therefore the acf's all have errors of less than a few percent. Note that if $d_v = 0$, then the errors vanish and the acf of V vanishes because $R_V(0^+) \propto d_v^2$.

III. BASE-BAND MIXERS

A base-band mixer multiplies the intermediate-frequency (IF) signal by 2 sinusoids whose phase difference is $\pi/2$ and whose frequencies are equal to the IF center frequency, thereby producing two slowly varying signals centered on zero frequency (base-band) which we call the real and imaginary parts of the base-band signal. The statistical properties of the base-band signal will be altered if the amplitudes and phases of the two sinusoids are not identical. If we let the amplitudes of the two sinusoids be $1 \pm \delta/2$ and the phase difference be $\pi/2 + \phi$ (instead of $\pi/2$), then the intensity modulation index will be, to lowest order in ϕ and δ ,

$$m_I = (\langle I^2 \rangle / \langle I \rangle^2 - 1)^{1/2} \approx 1 + (\delta^2 + \phi^2)/2. \quad (\text{A10})$$

Thus phase and amplitude errors only *increase* the intensity modulation index, because the number of degrees of freedom N is effectively decreased by mixer imperfections. We have assumed that the true ($\delta = \phi = 0$) base-band signal has real and imaginary parts that are zero-mean Gaussian random variables with equal variance. A sum of the squares of N such random variables will have a modulation index $m(N) = (2/N)^{1/2}$.

It can be shown that the mean values of the Stokes parameters will be altered by factors that are second-order or higher in the parameters δ and ϕ . Measurements of the modulation index of Gaussian noise at the output of the base-band mixers always satisfied $m_I \leq 1.01$. Therefore it is clear that errors in the measured Stokes parameters due to base-band mixer imperfections are always less than 1%.

REFERENCES

- Backer, D. C. 1970, *Nature*, **227**, 692.
 ———. 1973, *Ap. J.*, **182**, 245.
 Backer, D. C., Rankin, J. M., and Campbell, D. B. 1976, *Nature*, **263**, 202.
 Bergland, G. D. 1969, *IEEE Spectrum*, **6**, 41 (reprinted 1972 in *Digital Signal Processing*, ed. L. R. Rabiner and C. M. Rader [New York: IEEE Press], pp. 228–239).
 Blandford, R. D., and Scharlemann, E. T. 1976, *M.N.R.A.S.*, **174**, 59.
 Boriakoff, V. 1976, *Ap. J. (Letters)*, **208**, L43.
 Cocke, W. J., and Pacholczyk, A. G. 1976, *Ap. J. (Letters)*, **204**, L13.
 Cordes, J. M. 1975, *Ap. J.*, **195**, 193.
 ———. 1976a, *Ap. J.*, **208**, 944.
 ———. 1976b, *Ap. J.*, **210**, 780 (Paper I).
 Cordes, J. M., and Hankins, T. H. 1973, *Bull. AAS*, **5**, 18.
 Craft, H. D., Jr., Comella, J. M., and Drake, F. D. 1968, *Nature*, **218**, 1122.
 Hankins, T. H. 1971, *Ap. J.*, **169**, 487.
 ———. 1972, *Ap. J. (Letters)*, **177**, L11.
 ———. 1973, *Ap. J. (Letters)*, **181**, L49.
 Helfand, D. J., Manchester, R. N., and Taylor, J. H. 1975, *Ap. J.*, **198**, 661.
 Komesaroff, M., Morris, D., and Cooke, D. J. 1970, *Ap. Letters*, **5**, 37.
 Kraus, J. D. 1966, *Radio Astronomy* (New York: McGraw-Hill), p. 123.
 Lyne, A. G., Smith, F. G., and Graham, D. A. 1971, *M.N.R.A.S.*, **153**, 337.
 Manchester, R. N. 1971, *Ap. J. Suppl.*, **23**, 283.
 Manchester, R. N., Tademaru, E. H., Taylor, J. H., and Huguenin, G. R. 1973, *Ap. J.*, **185**, 951.

- Manchester, R. N., Taylor, J. H., and Huguenin, G. R. 1975, *Ap. J.*, **196**, 83.
- McCall, S. L., and Hahn, E. L. 1969, *Phys. Rev.*, **183**, 457.
- Rader, C. M. 1970, *IEEE Trans. Audio Electroacoust.*, **AU-18**, 439 (reprinted 1972 in *Digital Signal Processing*, ed. L. R. Rabiner and C. M. Rader [New York: IEEE Press], pp. 339-341).
- Radhakrishnan, V., and Cooke, D. J. 1969, *Ap. Letters*, **3**, 225.
- Rankin, J. M. 1973, personal communication.
- Rankin, J. M., Campbell, D. B., and Backer, D. C. 1974, *Ap. J.*, **188**, 608.
- Rankin, J. M., Campbell, D. B., and Spangler, S. R. 1975, *NAIC 46*, National Astronomy and Ionosphere Center, Arecibo, Puerto Rico.
- Rickett, B. J. 1975, *Ap. J.*, **197**, 185.
- Taylor, J. H., Huguenin, G. R., Hirsch, R. M., and Manchester, R. N. 1971, *Ap. Letters*, **9**, 205.
- Taylor, J. H., Manchester, R. N., and Huguenin, G. R. 1975, *Ap. J.*, **195**, 513.

J. M. CORDES: Department of Physics and Astronomy, Graduate Research Center, Tower B, University of Massachusetts, Amherst, MA 01002

T. H. HANKINS: National Astronomy and Ionosphere Center, Arecibo Observatory, Arecibo, PR 00612